available at www.sciencedirect.comjournal homepage: www.elsevier.com/locate/chnjc

Article (Dedicated to Professor Yi Chen on the occasion of his 80th birthday)

S-doped HTiNbO₅ nanosheets: A novel efficient visible-light photocatalyst

Lihong Zhang^a, Chenhui Hu^a, Liyuan Cheng^a, Weiping Ding^a, Wenhua Hou^{a,*}, Jing Chen^{b,#}^aKey Laboratory of Mesoscopic Chemistry of MOE, School of Chemistry and Chemical Engineering, Nanjing University, Nanjing 210093, Jiangsu, China^bSchool of Science, Nanjing University of Technology, Nanjing 211816, Jiangsu, China

ARTICLE INFO

Article history:

Received 22 June 2013

Accepted 26 August 2013

Published 20 November 2013

Keywords:

Titanoniobate nanosheet

Sulfur doping

Photodegradation

Rhodamine B

Visible light

ABSTRACT

S-doped HTiNbO₅ nanosheets were prepared via an exfoliation-flocculation-calcination process using layered HTiNbO₅ as the starting material and thiourea as the S source. The resulting catalyst had higher surface area and visible-light absorption than did unexfoliated HTiNbO₅ or HTiNbO₅ nanosheets. The adsorption and photodegradation of rhodamine B were evaluated under visible-light irradiation on the obtained catalysts. Both HTiNbO₅ nanosheets and S-doped HTiNbO₅ nanosheets showed enhanced adsorption capacity and a high visible-light photodegradation rate. However, a much higher degree of mineralization (41%) was achieved using the S-doped HTiNbO₅ nanosheets, compared with almost no mineralization for the HTiNbO₅ nanosheets, indicating that S doping can effectively improve the photocatalytic activity of nanosheets. The possible photodegradation mechanisms are also discussed.

© 2013, Dalian Institute of Chemical Physics, Chinese Academy of Sciences.

Published by Elsevier B.V. All rights reserved.

1. Introduction

Photocatalysis has been extensively studied in recent years because it is one of the most promising technologies for water purification and splitting [1]. TiO₂ has been widely investigated because of its various characteristics such as photostability, low price, and non-toxicity. However, effective photocatalysis on TiO₂ requires UV light [2,3]. Thus, developing novel efficient photocatalysts with visible-light response remains a great challenge in photodegradation [4,5].

Cation-exchanged layered transition-metal oxides, such as K₄Nb₆O₁₇, KNb₃O₈, K₄Ti₄O₉, and KTiNbO₅, have received enormous interest because of their wide variety of structural and electronic properties. In particular, their 2D structure can allow effective separation and transfer of photoinduced carriers in the interlayers [6]. Therefore, layered compounds now are

often used as efficient photocatalysts. Another very useful property of layered compounds is that they are amenable to delamination and reassembly, which may lead to the formation of corresponding nanosheets. H⁺-flocculated nanosheets exhibit not only a greatly increased surface area but also an enhanced protonic acidity because they contain more acid sites. These characteristics are very helpful for the adsorption and photodegradation of organic pollutants [7–10].

Layered compounds usually have a relatively wide band gap, and thus they are only photocatalytically active under UV light. To reduce the energy gap of layered transition-metal oxides, metallic elements such as Fe [11], Cr [12], and Ni [13], and nonmetallic elements such as C [14], N [15–20], P [21], and S [22–24] have been employed to tune the electronic structure of the layered compounds. The resultant catalysts showed good visible-light response and thus displayed a relatively high pho-

*Corresponding author. Tel: +86-25-83686001; Fax: +86-25-83317761; E-mail: whou@nju.edu.cn

#Corresponding author. Tel: +86-25-86206472; Fax: +86-25-83317761; E-mail: c1908@126.com

This work was supported by the National Basic Research Program of China (973 Program, 2009CB623504), the National Natural Science Foundation of China (21073084, 20773065), and the National Science Fund for Talent Training in Basic Science (J1103310).

DOI: 10.1016/S1872-2067(12)60692-5 | <http://www.sciencedirect.com/science/journal/18722067> | Chin. J. Catal., Vol. 34, No. 11, November 2013

tocatalytic activity under visible light. By comparison, nonmetal doping can not only tune the optical absorption edge of layered compounds to the visible-light region, but also prevent the recombination of photogenerated electron-hole pairs and also avoid secondary pollution from poisonous metal ions. Although there have been reports on the photocatalytic activity of layered transition-metal oxides doped with S [25–31], little attention has been given to S-doping of nanosheets made by exfoliation of layered transition-metal oxides.

In this work, a new way of doping HTiNbO₅ and its exfoliated derivative with S via an exfoliation-flocculation-calcination approach is presented. To prepare S-doped HTiNbO₅ nanosheets, HTiNbO₅ was first exfoliated with tetrabutylammonium hydroxide (TBAOH) to obtain nanosheets, which were then calcined with thiourea in air. For comparison, S-doped HTiNbO₅ was also prepared. The adsorption and visible-light photodegradation of rhodamine B (RhB) on the resulting catalysts were evaluated. Two different photodegradation mechanisms were proposed.

2. Experimental

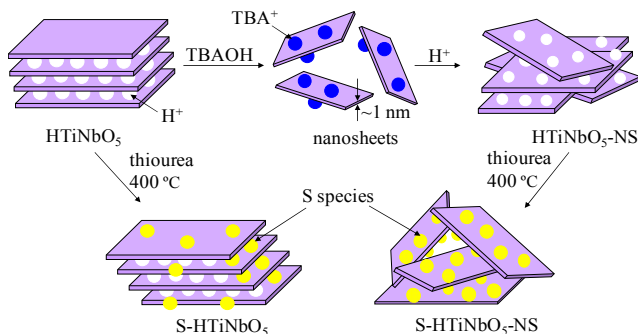
2.1. Catalyst preparation

Layered KTiNbO₅ was prepared by heating a stoichiometric mixture of K₂CO₃, Nb₂O₅, and TiO₂ at 1100 °C for 24 h. HTiNbO₅ was obtained by ion-exchange of KTiNbO₅ with HNO₃ (6 mol/L) at room temperature for 72 h [32]. HTiNbO₅ powder (1.0 g) was dispersed in 100 mL deionized water, and then 10 wt% of TBAOH was added until the pH reached 9–10. After stirring for 5 d, the supernatant solution containing [TiNbO₅]⁻ nanosheets was collected by centrifugation [33].

H⁺-reassembly of [TiNbO₅]⁻ nanosheets (to produce HTiNbO₅-NS) was carried out by the immediate aggregation of [TiNbO₅]⁻ nanosheets with HNO₃ (1 mol/L). The product was then washed thoroughly with deionized water and finally dried at 70 °C overnight. To prepare S-doped [TiNbO₅]⁻ nanosheets (S-HTiNbO₅-NS), HTiNbO₅-NS (1.0 g) was thoroughly mixed with thiourea (2.0 g) and then heated in air at 400 °C for 2 h. For comparison, S-doped HTiNbO₅ (S-HTiNbO₅) was prepared by using the same doping method but with unexfoliated HTiNbO₅ as starting material. The various preparation processes are shown in Scheme 1.

2.2. Catalyst characterization

X-ray diffraction (XRD) patterns of the resulting samples were recorded on a Philips X'Pert Pro X-ray diffractometer with Cu K_α radiation ($\lambda = 1.5418 \text{ \AA}$). The sample morphology was investigated by scanning electron microscopy (SEM, JEOL JEM-6300F). X-ray photoelectron spectroscopic (XPS) analysis was carried out on an X-ray photoelectron spectrometer (Thermo Fisher Scientific, K-Alpha) equipped with a hemispherical electron analyzer (pass energy of 20 eV) and an Al K_α ($h\nu = 1486.6 \text{ eV}$) X-ray source. The binding energies (BE) were referenced to the adventitious C 1s peak (284.6 eV), which was used as an internal standard to take into account charging ef-



Scheme 1. Procedures for the formation of exfoliated and H⁺-reassembled titanoniobate nanosheets and the corresponding S-doped catalysts.

fects. The BET specific surface area and BJH pore size distribution curves were obtained from N₂ adsorption-desorption isotherms determined at -196 °C on a Micromeritics ASAP 3020 surface area and porosity analyzer. Samples were degassed at 300 °C for 3 h prior to measurement. Ultraviolet-visible (UV-vis) diffuse reflectance spectra were obtained on a UV-vis spectrophotometer (Shimadzu, UV-2401) using BaSO₄ as a reference.

2.3. Adsorption and photocatalytic tests

RhB is one of the biodegradation-resistant N-containing dyes; there are two main methods used to remove or degrade it, physical adsorption and photodegradation. In this work, the adsorption capacity of the catalysts was determined as follows. Catalyst (0.150 g) was added into RhB solution (0.01 mmol/L, 100 mL), and the solution was then kept in the dark. At regular intervals, aliquots were sampled and centrifuged to obtain a transparent solution. The concentration of RhB remaining in the supernatant was determined by monitoring its UV-vis absorbance.

The photocatalytic activity was evaluated from the degradation of RhB under visible-light irradiation using a 300 W Xe lamp with a cutoff filter ($\lambda > 420 \text{ nm}$). A mixture of RhB solution (0.01 mmol/L, 100 mL) and catalyst (0.150 g) was first stirred well in the dark for a certain time to ensure that adsorption-desorption equilibrium was reached. Then the light was turned on. At given time intervals, the reaction suspension was sampled and centrifuged to remove the powders. The supernatants were analyzed by recording the absorbance at 553 nm using a UVmini-1240 (Shimadzu) spectrophotometer. The initial value of RhB concentration was assumed to be the adsorption-desorption equilibrium concentration determined previously. The degree of mineralization was followed by measuring the total organic carbon (TOC) content in the degraded solution using a TOC analyzer (Shimadzu, model TOC-5000) operated at a furnace temperature of 680 °C.

3. Results and discussion

3.1. XRD analysis

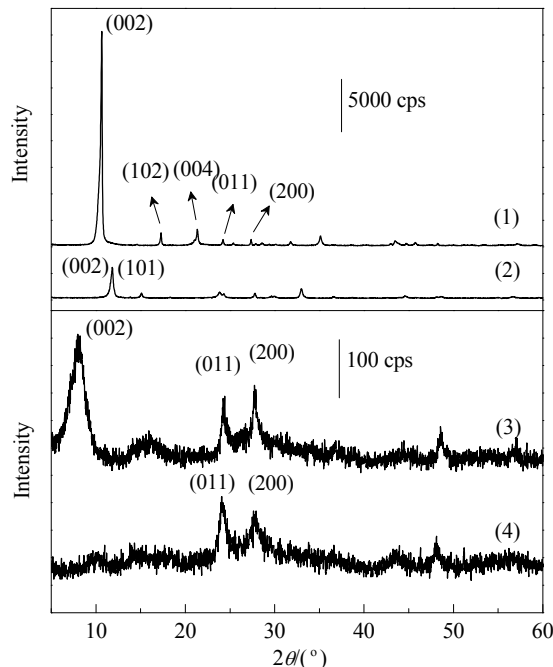


Fig. 1. XRD patterns of HTiNbO₅ (1), S-HTiNbO₅ (2), HTiNbO₅-NS (3), and S-HTiNbO₅-NS (4) samples.

Figure 1 shows XRD patterns of HTiNbO₅, HTiNbO₅-NS, S-HTiNbO₅, and S-HTiNbO₅-NS. The as-prepared HTiNbO₅ exhibits a sharp and strong characteristic (002) reflection at $2\theta = 10.6^\circ$, and the other reflections are well matched with the published data (PDF No. 75-2062), indicating a typical layered HTiNbO₅ structure. After heating HTiNbO₅ with thiourea in air at 400 °C, the characteristic (002) reflection remains, and the corresponding interlayer distance $d_{(002)}$ is decreased from 8.3 to 7.5 Å, indicating that calcination with thiourea has made the structure more compact.

After exfoliation of HTiNbO₅ with TBAOH and then reassembly with H⁺ ions, the resulting HTiNbO₅ nanosheets show a much weaker and broader (002) diffraction peak, indicating that HTiNbO₅-NS has a more disordered periodic layered structure than that of the original HTiNbO₅. Moreover, the characteristic (002) diffraction peak has shifted to a lower 2θ angle, and the corresponding interlayer spacing is increased from 8.3 to 11.0 Å. This suggests irregular restacking of titanoniobate nanosheets, which should help bulky molecules enter the layers.

After heating HTiNbO₅-NS with thiourea in air at 400 °C, the characteristic (002) diffraction peak is no longer observed. Nevertheless, in-plane diffractions are still present at $2\theta = 20^\circ$ –30°, showing that the basic slabs are retained although the layered structure is fully collapsed.

3.2. Morphology analysis

Figure 2 shows SEM images of HTiNbO₅, HTiNbO₅-NS, S-HTiNbO₅, and S-HTiNbO₅-NS samples. HTiNbO₅ has clear and regular layered structure with stacked flat layers. However, after reaction with TBAOH and then flocculation with H⁺ ions,

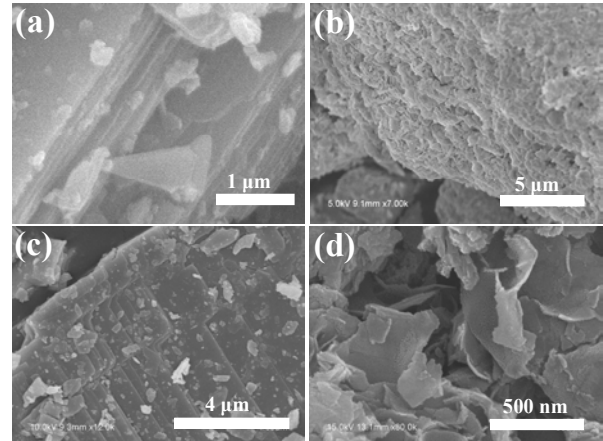


Fig. 2. SEM images of HTiNbO₅ (a), HTiNbO₅-NS (b), S-HTiNbO₅ (c), and S-HTiNbO₅-NS (d) samples.

the resulting HTiNbO₅-NS is rather disordered with loosely and irregularly piled-up titanoniobate nanosheets, indicating that exfoliation and flocculation can impair the interactions between the two layers and lead to a new arrangement of the nanosheets.

After heating HTiNbO₅ and HTiNbO₅-NS with thiourea at 400 °C, two distinctly different S-containing catalysts were obtained. S-HTiNbO₅ (Fig. 2(c)) has a clear layered structure with a step-and-platform morphology and a rather rough surface, while the layered structure of S-HTiNbO₅-NS has collapsed to give a layered structure of irregular lamellar plates with plicate edges. These findings agree well with the XRD results.

3.3. Surface area and porosity analysis

Figure 3 depicts N₂ adsorption-desorption isotherms and the corresponding BJH pore size distribution curves of HTiNbO₅-NS and S-HTiNbO₅-NS. Both samples have type IV isotherms along with H3-type hysteresis loops, indicating the presence of mesoporous structure (diameter range 2–50 nm). In addition, the two hysteresis loops shift close to $p/p_0 = 1$, suggesting that macropores larger than 50 nm are also present [34–36]. As shown in Fig. 3(b), HTiNbO₅-NS has a binodal pore size distribution with centers at 3.5 and 8.8 nm. After doping HTiNbO₅-NS with S, the centers of the corresponding binodal pore size distribution shift to ~3.8 and ~18.9 nm, respectively. According to the XRD and SEM results, the observed binodal pore size distribution can be attributed to the house-of-cards stacking structure and the space between the intercrossed [TiNbO₅]_n nanosheets. In comparison, S-HTiNbO₅-NS has a relatively broader pore size distribution and larger pores than HTiNbO₅-NS, indicating that S-doping can further enrich porosity.

Table 1 summarizes some structural aspects of S-doped and undoped HTiNbO₅ samples. The original HTiNbO₅ is nonporous with a surface area of only 3.7 m²/g. However, after exfoliation and flocculation, the surface area and pore volume of the resulting HTiNbO₅-NS are greatly increased. S doping further increases the surface area and pore volume of HTiNbO₅-NS. Among the four samples, S-HTiNbO₅-NS has the highest surface

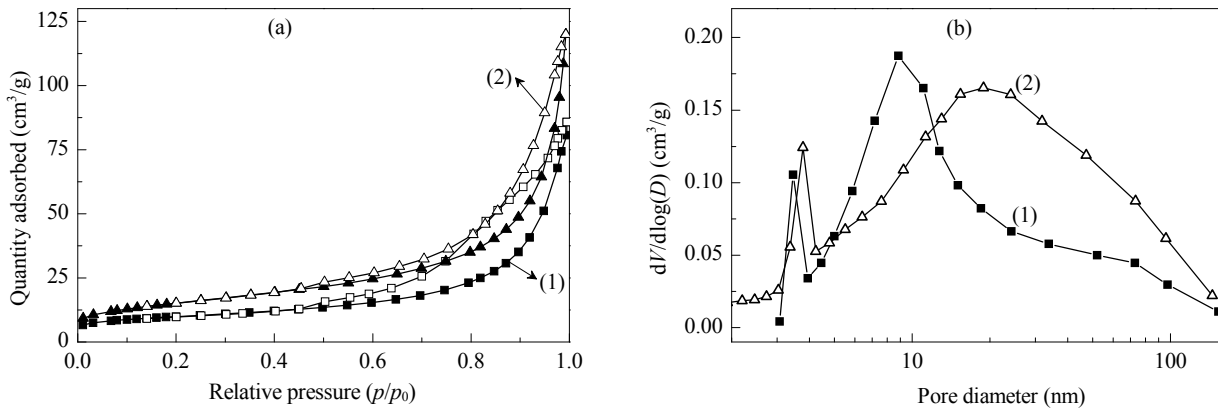


Fig. 3. Nitrogen adsorption-desorption isotherms (a) and pore size distribution curves (b) of HTiNbO₅-NS (1) and S-HTiNbO₅-NS (2) samples.

Table 1
Structural parameters of HTiNbO₅ and derivatives.

Sample	$d_{(002)}$ (nm)	S_{BET} (m ² /g)	Pore volume (cm ³ /g)	Pore diameter (nm)
HTiNbO ₅	0.83	3.7	—	—
S-HTiNbO ₅	0.75	7.6	—	—
HTiNbO ₅ -NS	1.06	41.7	0.13	3.5, 8.8
S-HTiNbO ₅ -NS	—	55.0	0.19	3.8, 18.9

area and pore volume; this can be attributed to both its rather irregularly piled-up titanoniobate nanosheets and the S doping. This larger surface area means that more SO₄²⁻ can be adsorbed. According to a previous report [37], the surface-adsorbed SO₄²⁻ can trap photoinduced electrons (e⁻), which is beneficial to photocatalytic activity.

3.4. XPS analysis

XPS measurements were performed to determine the environments and chemical states of S, Ti, and Nb in HTiNbO₅, S-HTiNbO₅, and S-HTiNbO₅-NS. The S 2p XPS spectra of S-HTiNbO₅-NS and S-HTiNbO₅ are displayed in Fig. 4(a). The binding energies (>168 eV) of S in the two catalysts are both assigned to sulfate species [38]. The S 2p binding energy of S-HTiNbO₅-NS shows two peaks at ~168.5 and ~169.7 eV, whereas S-HTiNbO₅ exhibits only one peak at ~168.8 eV. This

indicates that there is only one chemical environment for S in S-HTiNbO₅ but two in S-HTiNbO₅-NS. No signals are observed at 161–162 and 164 eV (where peaks would be expected for sulfide and elemental S [39]). However, there are other S 2p binding energies at 167.7 and 167.9 eV in S-HTiNbO₅-NS and S-HTiNbO₅, respectively. These peaks are from S⁶⁺ ions doped into the surface lattices of S-HTiNbO₅-NS and S-HTiNbO₅ [40–42].

As can be seen in Fig. 4(b) and (c), the Ti 2p and Nb 3d peaks of S-HTiNbO₅-NS are shifted to lower binding energies compared with those of HTiNbO₅, suggesting that there are relatively strong interactions between SO₄²⁻ and the nanosheets (Ti and Ti(Nb)), resulting in the increase of electron density around the Ti and Nb atoms. However, the Ti 2p and Nb 3d peaks of S-HTiNbO₅ are quite similar to those of HTiNbO₅, indicating that SO₄²⁻ has a relatively weaker interaction with HTiNbO₅. This may be because HTiNbO₅-NS has more acid sites and much stronger acidity than does neat HTiNbO₅, as a result of the exfoliation-flocculation process. This makes HTiNbO₅-NS react more readily with basic thiourea, leading to the formation of strong and effective bonds in S-HTiNbO₅-NS. According to the SEM and XPS results, the possible structures of the surface-adsorbed SO₄²⁻ in S-HTiNbO₅ and S-HTiNbO₅-NS are shown in Fig. 5. SO₄²⁻ are mainly located in the interlayers for S-HTiNbO₅ because of the periodic layered structure of the original HTiNbO₅, but are found on the basal planes of

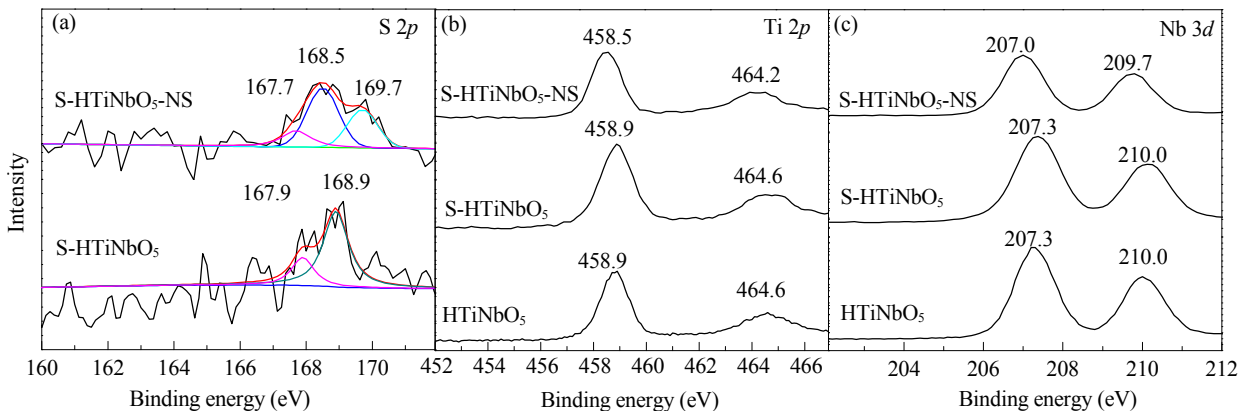


Fig. 4. XPS spectra of HTiNbO₅, S-HTiNbO₅, and S-HTiNbO₅-NS.

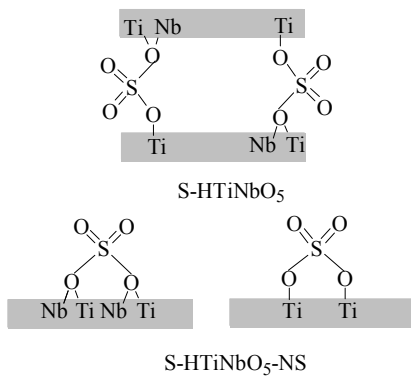


Fig. 5. A possible structure of the surface-adsorbed sulfate groups in S-HTiNbO₅ and S-HTiNbO₅-NS.

nanosheets in S-HTiNbO₅-NS because of the irregular and loose reassembly of HTiNbO₅-NS. As determined by XPS, the atomic concentrations of S in S-HTiNbO₅-NS and S-HTiNbO₅ are 0.68% and 0.39%, respectively. This difference is consistent with the larger surface area and stronger acidity of HTiNbO₅-NS [33]. In addition, S⁶⁺ ions doped into the surface lattice have a non-negligible impact on the decrease in Ti 2p binding energy in S-HTiNbO₅-NS. This is probably because of the difference in ionization energy between Ti and S [23,43].

3.5. UV-vis diffuse reflectance spectra analysis

Figure 6 shows UV-vis diffuse reflectance spectra of neat and S-doped catalysts. Both HTiNbO₅ and HTiNbO₅-NS exhibit clear absorption in the UV region (from the band-to-band transition) and no visible-light absorption. After S-doping, both S-HTiNbO₅ and S-HTiNbO₅-NS show a two-step absorption edge. The first absorption edge is clearly shifted towards the visible region and can be assigned to the intrinsic band-gap absorption. The second absorption in the visible-light region can be attributed to S-doping. By comparison, S-HTiNbO₅-NS has a much longer tail (420–800 nm) than S-HTiNbO₅ (420–520 nm). Compared with the undoped samples, the visible-light absorption of S-doped photocatalysts is enhanced, which can be attributed to the formation of localized energy

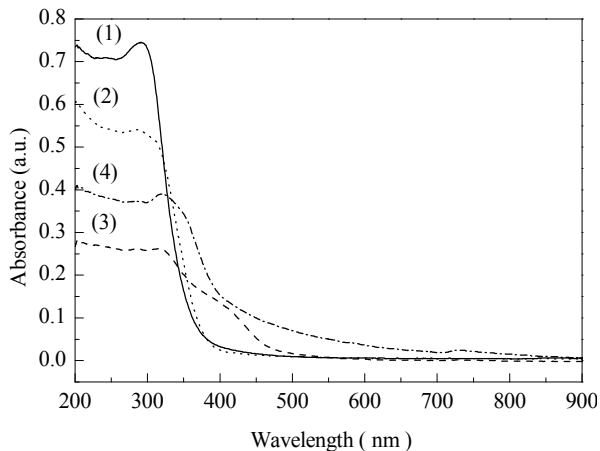


Fig. 6. UV-vis diffuse reflectance spectra of HTiNbO₅ (1), HTiNbO₅-NS (2), S-HTiNbO₅ (3), and S-HTiNbO₅-NS (4) samples.

levels [44].

3.6. Adsorption and photocatalytic activity

The adsorption capacities of the catalysts are shown in Fig. 7. The adsorption of RhB on these catalysts takes place in two stages. The first stage involves a rapid decrease in concentration, which plateaus within a short time (< 100 min); this can be attributed to physical adsorption and neutralization by the surface H⁺ of the catalysts. The second one is a gentle decrease in RhB concentration with time and can be attributed to the slow intercalation reaction driven by the basic nature of RhB. The times needed to reach adsorption-desorption equilibrium are about 20, 30, 50, and 70 min for HTiNbO₅, S-HTiNbO₅-NS, HTiNbO₅-NS, and S-HTiNbO₅, respectively. Of the catalysts, HTiNbO₅-NS has the largest physical adsorption capacity (~2.2 μmol/g), whereas S-HTiNbO₅-NS has the lowest one (~1.0 μmol/g) although with larger specific area and pore volume.

Compared with HTiNbO₅ and HTiNbO₅-NS, the corresponding S-doped versions exhibit slower intercalation after reaching physical adsorption-desorption equilibrium. This may be because of a decrease in the Brønsted acidity of the layers resulting from the replacement of H⁺ with SO₄²⁻ after calcination, leading to weaker interaction between the nanosheets and RhB. Only 40% of the RhB was intercalated into S-HTiNbO₅-NS even after 700 min, while nearly 50% was intercalated into HTiNbO₅-NS.

Figure 8 shows the photodegradation rates of RhB over the catalysts under visible light. Photodegradation of RhB is clearly negligible without any catalysts. By comparison, HTiNbO₅ produces almost 90% degradation of RhB within 50 min. For S-HTiNbO₅, only 30% of RhB was removed within 50 min. Because S-HTiNbO₅ was obtained through calcining HTiNbO₅

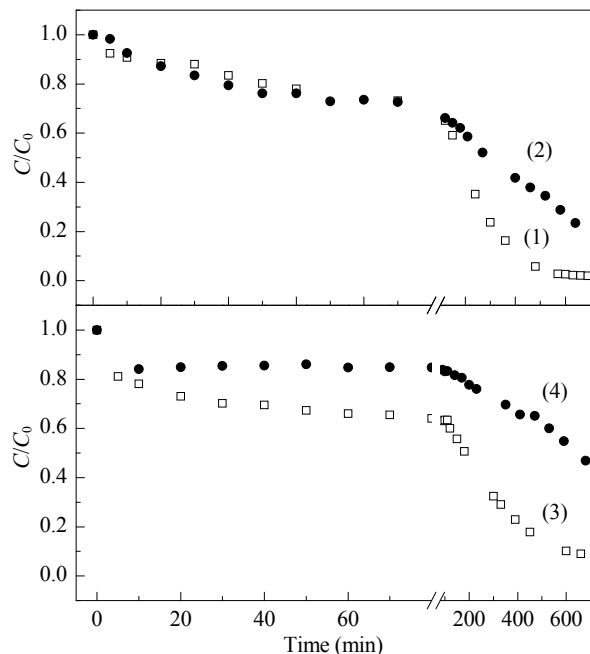


Fig. 7. Physical adsorption and intercalation of RhB by HTiNbO₅ (1), S-HTiNbO₅ (2), HTiNbO₅-NS (3), and S-HTiNbO₅-NS (4).

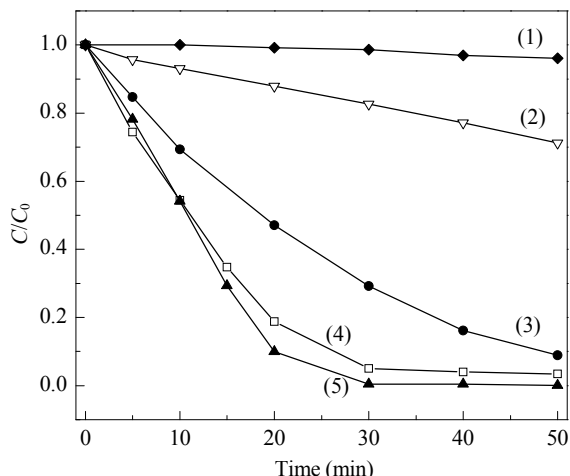


Fig. 8. Photocatalytic degradation of RhB under visible-light irradiation without catalyst (1) and with S-HTiNbO₅ (2), HTiNbO₅ (3), HTiNbO₅-NS (4) and S-HTiNbO₅-NS (5).

solid (acid) with thiourea (base), it is expected that the protonic acidity of S-HTiNbO₅ is less than that of HTiNbO₅, which weakens its ability to adsorb the basic dye RhB (see Fig. 7) and hence decreases the photocatalytic activity.

Interestingly, S-HTiNbO₅-NS and HTiNbO₅-NS exhibit faster photodegradation rates than S-HTiNbO₅ and HTiNbO₅. After 30 min of visible-light irradiation, approximately 95% RhB was degraded over HTiNbO₅-NS, but complete degradation of RhB was achieved over S-HTiNbO₅-NS samples.

Figure 9 shows UV-vis spectra and color changes of RhB aqueous solutions in the presence of different HTiNbO₅ sam-

ples under visible-light irradiation. The intensity of the characteristic peak at 553 nm from the RhB chromophores is decreased rapidly by both HTiNbO₅-NS and S-HTiNbO₅-NS catalysts and more slowly for HTiNbO₅ and S-HTiNbO₅, in good agreement with the changes in color of the RhB aqueous solutions. Both the dye chromophores and aromatic rings of RhB have been destroyed within 50 min over S-HTiNbO₅-NS, indicating that the dye molecules had been degraded, not just decolorized.

TOC analysis was carried out to determine the degree of mineralization of RhB because decolorization does not necessarily mean that RhB has been completely oxidized into harmless final products such as H₂O and CO₂. The TOC value of the RhB solution catalyzed by S-HTiNbO₅-NS was decreased by approximately 41.0% while that of the solution over HTiNbO₅-NS was essentially unchanged after 50 min, although their color removal values were over 96% and 99%, respectively. This implies that RhB is mainly degraded into aliphatic organic compounds over HTiNbO₅-NS but is partially mineralized further over S-HTiNbO₅-NS, revealing that S doping can improve the photocatalytic activity of HTiNbO₅-NS.

3.7. Photocatalytic mechanism

To elucidate the photocatalytic mechanism, it is important to detect hole oxidative species in the photodegradation process. As we know, EDTA-2Na is an effective hole scavenger for photocatalytic reactions [45]. As shown in Fig. 10, the photocatalytic degradation efficiency of RhB catalyzed by S-HTiNbO₅-NS significantly decreased in the presence of EDTA-2Na (1 mmol/L), while the degradation rate of RhB over HTiNbO₅-NS

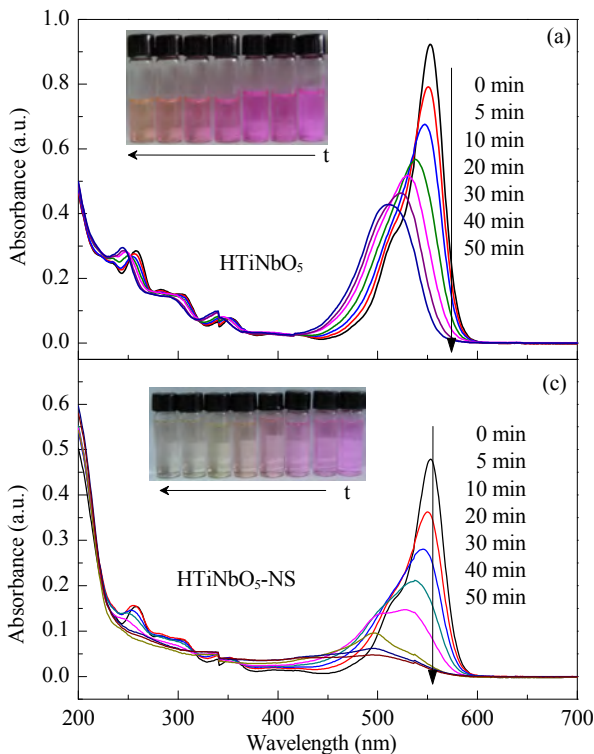
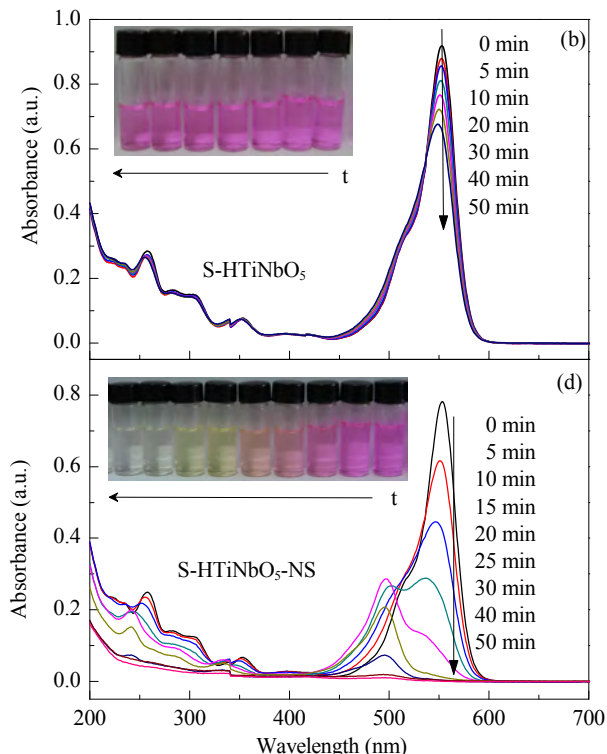


Fig. 9. UV-vis spectra and color changes of RhB aqueous solutions under visible-light irradiation in the presence of HTiNbO₅ (a), S-HTiNbO₅ (b), HTiNbO₅-NS (c), and S-HTiNbO₅-NS (d) samples.



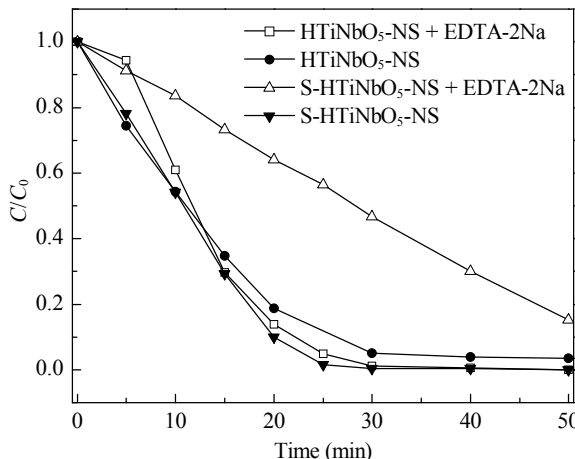


Fig. 10. Photocatalytic degradation of RhB in the presence of EDTA-2Na (1 mmol/L).

remained nearly unchanged. This means that photogenerated holes existed during the photodegradation of RhB over S-HTiNbO₅-NS, making this degradation different from the photosensitization occurred on HTiNbO₅-NS.

According to the previous literature [47], no holes in the valence band of the semiconductor are involved during the photosensitization process. However, in the photocatalytic process, the primary oxidative species are photogenerated holes. These holes can oxidize H₂O to •OH or directly oxidize organic pollutants. Because of the strong oxidizing power, holes and •OH can make mineralization complete.

Based on our results, we propose two possible photodegradation mechanisms as illustrated in Fig. 11. For HTiNbO₅-NS, which only has UV absorption, the degradation process of RhB under visible-light irradiation is expected to be photosensitized oxidation (Fig. 11(a)). In this process, RhB molecules are adsorbed onto the surface of the catalyst and excited by harvesting visible light. Next, the excited-state electrons are immediately transferred into the conduction band of the catalyst and

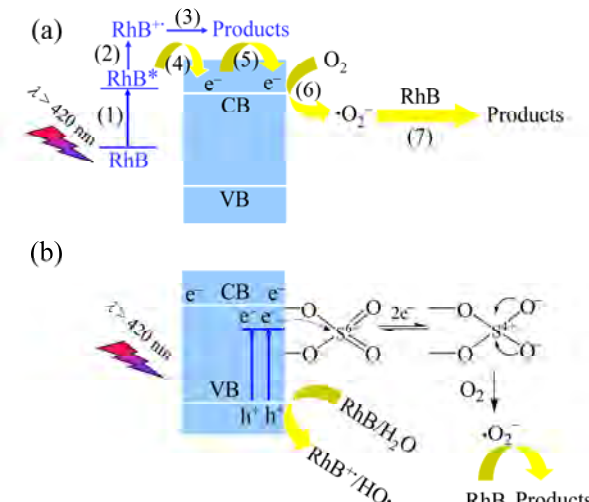


Fig. 11. Possible mechanisms for the photodegradation of RhB under visible-light irradiation by HTiNbO₅-NS (a) and S-HTiNbO₅-NS (b).

react with adsorbed oxygen to generate reactive O species such as •O₂[−], ultimately leading to the degradation of RhB [47].

In contrast, the main mechanism of photodegradation over S-HTiNbO₅-NS was photocatalysis, along with photosensitized oxidation. As shown in Fig. 11(b), because of the doping of S into the surface lattice of the catalyst, additional electronic states would be formed below the conduction band edge, giving rise to the visible-light response [37,46,48]. Besides this, surface-adsorbed SO₄^{2−} could capture photoinduced electrons and thus protect the photoinduced holes [49].

4. Conclusions

S-HTiNbO₅-NS has been successfully synthesized via an exfoliation-flocculation-calcination method using thiourea as the S source. The S-HTiNbO₅-NS exhibited not only a large specific surface area and rich mesoporosity, but also good absorption of visible light. S species exist as S⁶⁺ ions in the surface lattice and SO₄^{2−} adsorbed on the surface, respectively. The former may lead to the visible-light absorption while the latter suppresses the recombination of photogenerated electrons and holes. S-HTiNbO₅-NS can be used as an effective catalyst for visible-light photodegradation of RhB aqueous solution through the synergistic effect of the two kinds of S species. This method is an excellent strategy to enhance the photocatalytic activity of nanosheets peeled from layered transition-metal oxides, and should provide new opportunities for the fabrication of highly-effective visible-light-driven photocatalysts.

References

- [1] Hoffmann M R, Martin S T, Choi W, Bahnemann D W. *Chem Rev*, 1995, 95: 69
- [2] Chen X B, Shen S H, Guo L J, Mao S S. *Chem Rev*, 2010, 110: 6503
- [3] Fujishima A, Rao T N, Tryk D A. *J Photochem Photobiol C*, 2000, 1: 1
- [4] Li Q, Guo B D, Yu J G, Ran J R, Zhang B H, Yan H J, Gong J R. *J Am Chem Soc*, 2011, 133: 10878
- [5] Zhang J, Yu J G, Zhang Y M, Li Q, Gong J R. *Nano Lett*, 2011, 11: 4774
- [6] Takata T, Tanaka A, Hara M, Kondo J N, Domen K. *Catal Today*, 1998, 44: 17
- [7] Yang G, Hou W H, Feng X M, Jiang X F, Guo J. *Adv Funct Mater*, 2007, 17: 3521
- [8] Allen M R, Thibert A, Sabio E M, Browning N D, Larsen D S, Osterloh F E. *Chem Mater*, 2010, 22: 1220
- [9] Yang G, Hou W H, Feng X M, Xu L, Liu Y G, Wang G, Ding W P. *Adv Funct Mater*, 2007, 17: 401
- [10] He J, Li Q J, Tang Y, Yang P, Li A, Li R, Li H Z. *Appl Catal A*, 2012, 443-444: 145
- [11] Kim T W, Ha H W, Paek M J, Hyun S H, Baek I H, Choy J H, Hwang S J. *J Phys Chem C*, 2008, 112: 14853
- [12] Kim T W, Hur S G, Hwang S J, Park H, Choi W, Choy J H. *Adv Funct Mater*, 2007, 17: 307
- [13] Kim T W, Hwang S J, Jhung S H, Chang J S, Park H, Choi W, Choy J H. *Adv Mater*, 2008, 20: 539
- [14] Leary R, Westwood A. *Carbon*, 2011, 49: 741
- [15] Asahi R, Morikawa T, Ohwaki T, Aoki K, Taga Y. *Science*, 2001, 293: 269
- [16] Li X K, Kikugawa N, Ye J H. *Adv Mater*, 2008, 20: 3816

Graphical Abstract

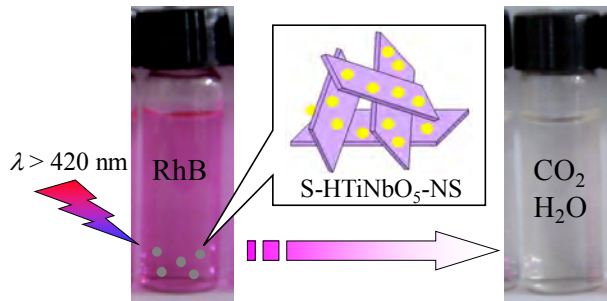
Chin. J. Catal., 2013, 34: 2089–2097 doi: 10.1016/S1872-2067(12)60692-5

S-doped HTiNbO₅ nanosheets: A novel efficient visible-light photocatalyst

Lihong Zhang, Chenhui Hu, Liyuan Cheng, Weiping Ding,
Wenhua Hou*, Jing Chen*

Nanjing University; Nanjing University of Technology

S-doped HTiNbO₅ nanosheets have increased surface area and clear visible-light absorption. These catalysts showed a high visible-light photodegradation rate and a relatively high mineralization degree of 41%, indicating that S doping can effectively improve the photocatalytic activity of nanosheets.



- [17] Zheng Z, Huang Y C, Xu L, Yang X Y, Hu C H, Zhang L H, Fan Y N, Hou W H. *Nano Res*, 2011, 4: 635
- [18] Zhai Z, Yang X Y, Xu L, Hu C H, Zhang L H, Hou W H, Fan Y N. *Nanoscale*, 2012, 4: 547
- [19] Zhai Z, Hu C H, Yang X Y, Zhang L H, Liu C, Fan Y N, Hou W H. *J Mater Chem*, 2012, 22: 19122
- [20] Liu G, Yang H G, Wang X W, Cheng L N, Pan J, Lu G Q, Cheng H M. *J Am Chem Soc*, 2009, 131: 12868
- [21] Zheng R Y, Lin L, Xie J L, Zhu Y X, Xie Y C. *J Phys Chem C*, 2008, 112: 15502
- [22] Li H X, Zhang X Y, Huo Y N, Zhu J. *Environ Sci Technol*, 2007, 41: 4410
- [23] Liu S X, Chen X Y. *J Hazard Mater*, 2008, 152: 48
- [24] Tian H, Ma J F, Li K, Li J J. *Ceram Int*, 2009, 35: 1289
- [25] Liu J W, Wang L, Liu J H, Wang T C, Qu W L, Li Z H. *Cent Eur J Phys*, 2009, 7: 762
- [26] Huo G Y, Ren X, Qian L L, Zhang N, Liu S, Yan X. *J Magn Magn Mater*, 2013, 343: 119
- [27] Dhanasekaran P, Gupta N M. *Int J Hydrogen Energy*, 2012, 37: 4897
- [28] Liu P, Nisar J, Pathak B, Ahuja R. *Int J Hydrogen Energy*, 2012, 37: 11611
- [29] Marschall R, Mukherji A, Tanksale A, Sun C H, Smith S C, Wang L Z, Lu G Q. *J Mater Chem*, 2011, 21: 8871
- [30] Nisar J, Pathak B, Wang B C, Kang T W, Ahuja R. *Phys Chem Chem Phys*, 2012, 14: 4891
- [31] Zhang C, Jia Y Z, Jing Y, Yao Y, Ma J, Sun J H. *Phys B*, 2012, 407: 4649
- [32] Hou W H, Ma J, Yan Q J, Fu X C. *J Chem Soc, Chem Commun*, 1993: 1144
- [33] Takagaki A, Sugisawa M, Lu D, Kondo J N, Hara M, Domen K, Hayashi S. *J Am Chem Soc*, 2003, 125: 5479
- [34] Yu J G, Guo H T, Davis S A, Mann S. *Adv Funct Mater*, 2006, 16: 2035
- [35] Bavykin D V, Parmon V N, Lapkin A A, Walsh F C. *J Mater Chem*, 2004, 14: 3370
- [36] Yu J, Yu H, Cheng B, Traplis C. *J Mol Catal A*, 2006, 249: 135
- [37] Niu Y X, Xing M Y, Tian B Z, Zhang J L. *Appl Catal B*, 2012, 115-116: 253
- [38] Colón G, Hidalgo M C, Munuera G, Ferino I, Cutrufello M G, Navío J A. *Appl Catal B*, 2006, 63: 45
- [39] Boudali L K, Ghorbel A, Grange P, Figueras F. *Appl Catal B*, 2005, 59: 105
- [40] Ohno T, Akiyoshi M, Umebayashi T, Asai K, Mitsui T, Matsumura M. *Appl Catal A*, 2004, 265: 115
- [41] Rengifo-Herrera J A, Mielczarski E, Mielczarski J, Castillo N C, Kiwi J, Pulgarin C. *Appl Catal B*, 2008, 84: 448
- [42] Fang J, Shi F C, Bu Jing, Ding J J, Xu S T, Bao J, Ma Y S, Jiang Z Q, Zhang W P, Gao C, Huang W X. *J Phys Chem C*, 2010, 114: 7940
- [43] Znad H, Kawase Y. *J Mol Catal A*, 2009, 314: 55
- [44] Bidaye P P, Khushalani D, Fernandes J B. *Catal Lett*, 2010, 134: 169
- [45] Lv Y H, Pan C S, Ma X G, Zong R L, Bai X J, Zhu Y F. *Appl Catal B*, 2013, 138-139: 26
- [46] Liu G, Wang L Z, Yang H G, Cheng H M, Lu G Q. *J Mater Chem*, 2010, 20: 831
- [47] Chen C C, Ma W H, Zhao J C. *Chem Soc Rev*, 2010, 39: 4206
- [48] Chen X B, Burda C. *J Am Chem Soc*, 2008, 130: 5018
- [49] Li H X, Li G S, Zhu J, Wan Y. *J Mol Catal A*, 2005, 226: 93

S掺杂的HTiNbO₅纳米片：一种新型高效可见光催化剂

张丽宏^a, 胡晨晖^a, 程立媛^a, 丁维平^a, 侯文华^{a,*}, 陈 静^{b,#}

^a南京大学化学与化工学院, 介观化学教育部重点实验室, 江苏南京210093

^b南京工业大学理学院, 江苏南京211816

摘要: 将层状HTiNbO₅剥层絮凝成HTiNbO₅纳米片, 然后与硫脲焙烧, 制得了S掺杂的HTiNbO₅纳米片。与原始HTiNbO₅和HTiNbO₅纳米片相比, 该样品具有较大的比表面积和明显的可见光吸收。以罗丹明B为降解物, 评价了该催化剂的吸附性能和可见光催化性能。结果表明, HTiNbO₅纳米片和S掺杂的HTiNbO₅纳米片都具有很好的吸附能力和很高的可见光降解速率。然而, 对于罗丹明B的矿化, S掺杂的HTiNbO₅纳米片可以达到41%矿化率, 而HTiNbO₅纳米片上矿化率几乎为零。这说明S掺杂能有效改善纳米片的光催化效果。最后, 对可能的光催化机理进行了探讨。

关键词: 钛铌酸纳米片; 硫; 掺杂; 光降解; 罗丹明B; 可见光

收稿日期: 2013-06-22. 接受日期: 2013-08-26. 出版日期: 2013-11-20.

*通讯联系人. 电话: (025)83686001; 传真: (025)83317761; 电子信箱: whou@nju.edu.cn

#通讯联系人. 电话: (025)86206472; 传真: (025)83317761; 电子信箱: cj1908@126.com

基金来源: 国家重点基础研究发展计划(973计划, 2009CB623504); 国家自然科学基金(21073084, 20773065); 国家基础科学人才培养基金(J1103310).

本文的英文电子版由Elsevier出版社在ScienceDirect上出版(<http://www.sciencedirect.com/science/journal/18722067>).

2012 年国内化学类期刊影响因子和总被引频次排序表

(据中国科学技术信息研究所 2013 年 9 月 27 日发布的《2013 年版中国科技期刊引证报告(核心版)》)

期刊名称	影响因子		总被引频次		期刊名称	影响因子		总被引频次	
	数值	排名	数值	排名		数值	排名	数值	排名
色谱	1.382	1	2312	6	分子科学学报	0.532	18	259	30
分析化学	1.267	2	4015	1	Chinese Chemical Letters	0.493	19	1072	16
催化学报	1.198	3	2220	7	分析科学学报	0.478	20	914	18
高等学校化学学报	1.020	4	3949	2	影像科学与光化学	0.475	21	200	33
物理化学学报	0.999	5	2846	3	质谱学报	0.467	22	410	26
分析测试学报	0.976	6	2091	8	应用化学	0.464	23	1387	13
高分子学报	0.968	7	1549	12	功能高分子学报	0.438	24	480	23
分子催化	0.934	8	675	20	电化学	0.376	25	255	31
无机化学学报	0.845	9	2313	5	化学研究与应用	0.340	26	1009	17
有机化学	0.745	10	1580	11	化学研究	0.334	27	315	27
化学学报	0.701	11	2680	4	化学通报	0.332	28	898	19
化学进展	0.695	12	1726	10	化学分析计量	0.274	29	411	25
Chinese Journal of Polymer Science	0.673	13	274	29	核化学与放射化学	0.265	30	208	32
分析试验室	0.616	14	1892	9	合成化学	0.245	31	433	24
中国科学化学	0.555	15	1193	14	Chinese Journal of Chemical Physics	0.226	32	288	28
Chemical Research in Chinese Universities	0.549	16	569	22	化学试剂	0.215	33	648	21
高分子通报	0.536	17	1108	15					